Pattern Recognition Letters 31 (2010) 143–150

Contents lists available at ScienceDirect

Pattern Recognition Letters

journal homepage: www.elsevier.com/locate/patrec

Fast and accurate method for radial moment's computation

Khalid M. Hosny *

Department of Information Technology, Faculty of Computers and Informatics, Zagazig University, Zagazig, Egypt

ARTICLE INFO

Article history:
Received 30 November 2008
Received in revised form 7 July 2009
Available online 3 October 2009

Communicated by J.A. Robinson

Keywords:
Radial moments
Geometric moments
Exact computation
Circularly moments
Symmetry property

ABSTRACT

Fast and accurate method is proposed for radial moment's computation. Exact radial moments are computed as a linear combination of exact geometric moments. The digital image is transformed to be inside the unit circle, where the transformed image is divided into four quadrants. Based on the symmetry property; only one quadrant of transformed image is needed to compute the whole set of moments. This leads to significant reduction in the computational complexity requirements. The proposed method completely removes the approximation errors and tremendously reduced the computational demands. Numerical experiments are performed, where the obtained results are compared with the approximated values. The obtained results clearly explained the efficiency of the proposed method.

1. Introduction

Circularly orthogonal moments, such as Zernike, Pseudo-Zernike and Fourier-Mellin moments are generally used to represent an image with the minimum amount of information redundancy (Teague, 1980). In addition to this attractive property, the set of circularly orthogonal moments are rotation and flipping invariants by nature, while the translation and scale invariants are easily achieved through the normalization of their polynomials. Based on their attractive characteristics, circularly orthogonal moments are widely used in image processing, pattern recognition and computer vision. Circularly orthogonal moments are used as invariant pattern or object recognition (Khotanzad and Hong, 1990; Wang and Healey, 1998; Kan and Srinath, 2002; Broumandnia and Shanbehzadeh, 2007), content-based image retrieval (Kim and Kim, 1998), watermarking and data-hiding (Kim and Lee, 2003; Xin et al., 2004; Amin and Subhulukshini, 2004), edge detection (Ghosal and Mehrotra, 1992; Dong et al., 2005; Bin et al., 2008), image segmentation (Ghosal and Mehrotra, 1993), biomedical engineering (Iskander et al., 2001, 2002), medical imaging (Bharathi and Ganesan, 2008), and face recognition (Haddadnia et al., 2003; Kim and Kim, 2008; Kanan and Faez, 2009).

Radial moment's computation is the main part of the computational process of these orthogonal moments, where all of these moments could be expressed as linear combinations of radial moments. Approximate computation of radial moments produced numerical instabilities and consequently degraded the quality of the computed descriptors.

Digital images are usually defined in the Cartesian coordinates while the circular moments are by nature defined in the polar coordinates. Consequently, computation of these circular moments required square-to-circle transformation which produced what is called geometric error. The other kind of error is the numerical error which is the direct result of approximation process. Zernike (ZMs) and Pseudo-Zernike moments (PZMs) could be expressed as a linear combination of radial or geometric moments of the same order or less (Teh and Chin, 1988). Orthogonal Fourier-Mellin moments (OFMMs) were defined first by Sheng and Shen (1994). Similar to ZMs and PZMs, OFMMs could be expressed as a linear combination of radial or geometric moments. It is clear that, the computational accuracy of all the aforementioned circularly orthogonal moments is dependent on the computational accuracy of the radial moments.

Recently Wee and Paramesran (2006), proposed a method that compute approximate radial moments using symmetry property. In fact, their method reduces the computational complexity requirements but on the other side it produces a set of approximate radial moments, where the numerical error problem is still unsolved.

Apart from the circular orthogonal moments, other orthogonal moments like Legendre, Gegenbauer, Tchebichef and Krawtchouk moments could be expressed as a linear combination of only geometric moments of the same order or less. Also Novotni and Klein (2004) shows that 3D Zernike moments could be expressed as a combination of geometric moments. Therefore, the implementation

* Current address: Department of Computer Science, Najran Community College, Najran University, P.O. Box 1988, Najran, Saudi Arabia. Tel.: +966 055 3517581; fax: +966 07 5440357.
E-mail address: k_hosny@yahoo.com.

0167-8655/$ - see front matter © 2009 Elsevier B.V. All rights reserved.
doi:10.1016/j.patrec.2009.09.027

of symmetrical property to radial moment's computation as done by Wee and Paramesran (2006) limited its benefit to circular orthogonal moments, while, its implementation to geometric moment's computation make it useful in the computation of all orthogonal moments and their extension to three-dimension. This is the motivation of this work, where the symmetrical property is implemented in the process of exact geometric moment's computation.

This paper proposes a new method for accurate computation of radial moments for gray-level images and objects. The radial moments are computed exactly as a linear combination of exact geometric moments, while the later are computed exactly by using a mathematical integration of the monomial polynomials. The symmetry property and fast algorithm are applied for computational complexity reduction. Experimental results clearly show the efficiency of this proposed method.

The rest of the paper is organized as follows: in Section 2, an overview of the radial moments is presented. The proposed method is described in Section 3. Section 4 is devoted to numerical experiments. Conclusion and concluding remarks are presented in Section 5.

2. Radial moments

Radial or rotational moments of order p and repetition q are defined as:

$$R_{pq} = \int_0^{2\pi} \int_0^1 r^p e^{-\hat{i}q\theta} f(r\cos\theta, r\sin\theta) r dr d\theta, \tag{1}$$

where $\hat{i} = \sqrt{-1}, p = 0, 1, 2, 3, \ldots, \infty$ and q is any positive or negative integer. Based on Eq. (1), radial moments are defined in terms of polar coordinates (r, θ) over a unit disk. On the other side, image intensity function defined in Cartesian coordinates (x,y). Consequently, an appropriate image mapping is imperative. There are mainly two traditional mapping approaches. In the first approach, the square image plane is mapped onto a unit disk, where the center of the image is assumed to be the origin of coordinates. In this approach, all pixels outside the unit disk are ignored, which results in a loss of some image information. In the second approach, the whole square image is mapped inside the unit disk, where the center of the image is assumed to be the coordinate origin. The second approach overcomes the lost information problem in the first kind of transformation.

For a digital image of size $N \times N$ the integrals in Eq. (1) are replaced by summations and the image is normalized inside the unit disk using second aforementioned mapping transformations. The approximated radial moments are:

$$\widetilde{R}_{pq} = \lambda_p \sum_{i=0}^{N-1} \sum_{i=0}^{N-1} r_{ij}^p e^{-\hat{i}q\theta_{ij}} f(i,j). \tag{2}$$

Eq. (2) is so-called direct method for radial moment's computation, which is the approximated version using zeroth-order approximation (ZOA). λ_p is the total number of pixels that achieve the condition $|r_{ij}| \leqslant 1$. This equation has two sources of errors, the first one is the numerical error and the other is the geometrical error. The numerical error is caused by approximating integrals in Eq. (1) through replacing them by summations. Based on the principles of mathematical analysis, summations are equivalent to integrals as the number of sampling points tends to infinity. Consequently, the numerical error increases as the number of sampling points decreases. Also, this error increases as the order of moments increases. Therefore, numerical instabilities are faced when the moment order reaches a certain value. The geometrical error is caused by a square to circular mapping transformation.

2.1. Circular orthogonal moments via radial moments

Circular orthogonal moments are represented as a linear combination of radial moments of the same order or less. Relations of ZMs, PZMs and OFMMs with radial moments are briefly discussed through the following subsections.

2.1.1. Zernike moments

The complex two-dimensional Zernike moments of order p and repetition q are defined as a linear combination of radial moments as follows:

$$Z_{pq} = \frac{p+1}{\pi} \sum_{\substack{k=q \\ p-k=\text{even}}}^{p} B_{pqk} R_{kq}, \tag{3}$$

where $p = 0, 1, 2, 3, \ldots, \infty$ and q is positive integer according to the conditions $p - q$ = even, $q \leqslant p$. Zernike moments with negative values of repetition q are obtained directly by making use of the complex conjugate of Zernike moments in Eq. (3). The coefficient matrix B_{pqk} is defined as:

$$B_{pqk} = \frac{(-1)^{\left(\frac{p-k}{2}\right)} \left(\frac{p+k}{2}\right)!}{\left(\frac{p-k}{2}\right)! \left(\frac{k+q}{2}\right)! \left(\frac{k-q}{2}\right)!} \tag{4}$$

and recursively computed through the following relations:

$$B_{ppp} = 1, \tag{5.1}$$

$$B_{p(q-2)p} = \frac{p+q}{p-q+2} B_{pqp}, \tag{5.2}$$

$$B_{pq(k-2)} = -\frac{(k+q)(k-q)}{(p+k)(p-k+2)} B_{pqk}. \tag{5.3}$$

2.1.2. Pseudo-Zernike moments

Pseudo-Zernike moments of order p and repetition q are defined as a linear combination of radial moments as follows:

$$A_{pq} = \frac{p+1}{\pi} \sum_{k=q}^{p} C_{pqk} R_{kq}, \tag{6}$$

where the coefficient matrix C_{pqk} is defined as:

$$C_{pqk} = \frac{(-1)^{(p-k)}(p+k+1)!}{(p-k)!(k+q+1)!(k-q)!}. \tag{7}$$

Similar to the previous case, this matrix could be computed through the following recurrence relations:

$$C_{ppp} = 1, \tag{8.1}$$

$$C_{p(q-1)k} = \frac{k+q+1}{k-q+1} C_{pqk}, \tag{8.2}$$

$$C_{pq(k-1)} = -\frac{(k+q+1)(k-q+1)}{(p+k+1)(p-k+1)} B_{pqk}. \tag{8.3}$$

2.1.3. Fourier-Mellin moments

Orthogonal Fourier-Mellin moments of order p and repetition q are defined as a linear combination of radial moments as follows:

$$O_{pq} = \frac{p+1}{\pi} \sum_{k=0}^{p} \alpha_{pk} R_{kq}, \tag{9}$$

where the coefficient matrix $\alpha_{p\ k}$ is defined as:

$$\alpha_{pk} = \frac{(-1)^{(p+k)}(p+k+1)!}{(p-k)!k!(k+1)!}. \tag{10}$$

This matrix is computed using the following equations:

$$\alpha_{p0} = (-1)^p(p+1), \tag{11.1}$$

$$\alpha_{pk} = -\frac{(p+k+1)(p-k+1)}{k(k+1)}\alpha_{p(k-1)}. \tag{11.2}$$

3. The proposed method

The proposed method aims to provide a fast computation of exact radial moments. In addition to these elegant characteristic, the proposed method is a low-complexity method where it reduces the requirements by 75%. Through the next subsection, all these characteristics will be discussed in details.

3.1. Symmetry property

A digital image of size $N \times N$ is an array of pixels. The centers of these pixels are the points (x_i,y_j), where the image intensity function is defined only for this discrete set of points $(x_i,y_j) \in [0,N-1] \times [0,N-1]$. $\Delta x_i = x_{i+1} - x_i$, $\Delta y_j = y_{j+1} - y_j$ are sampling intervals in the x- and y-directions, respectively. The second square-to-circle mapping approach is applied as shown in Fig. 1, where the transformed coordinates are:

$$x_i = \frac{2i-N-1}{N\sqrt{2}}, \quad y_j = -\frac{2j-N-1}{N\sqrt{2}}, \tag{12.1}$$

$$r_{ij} = \sqrt{(x_i)^2 + (y_j)^2}, \quad \theta_{ij} = \tan^{-1}\left(\frac{y_j}{x_i}\right) \tag{12.2}$$

with $i = 1,2,\ldots,N$ and $j = 1,2,\ldots,N$.

The transformed image is inside the unit circle. The center of this image coincides with the Cartesian coordinate origin. Both axes divide the transformed image into four quadrants. Each point P_1 with the Cartesian coordinates (x_i,y_j) in the first quadrant which has three similar points in the other three quadrants as shown in Fig. 2. These points are $P_2(x_{N-i+1},y_j)$, $P_3(x_{N-i+1}, y_{N-j+1})$ and $P_4(x_i,y_{N-j+1})$. All of these four points have the same radial distance from the origin point as shown in Fig. 3.

The geometric moments of the order $(p+q)$ are the projection of the image function $f(x,y)$ onto the monomial x^py^q and defined as:

$$M_{pq} = \int_{-\infty}^{\infty}\int_{-\infty}^{\infty} x^p y^q f(x,y)dxdy. \tag{13}$$

Since the points P_1, P_2, P_3 and P_4 has the same radial distance, then; the numerical value of x^py^q will be dependent on whatever p and q are even or odd. For more clarification, we consider the following illustrative example. Assume the first point P_1 has the coordinates $P_1(x_7,y_3) = P_1\left(5/8\sqrt{2}, 3/8\sqrt{2}\right)$. Consequently, the coordinates of the other three points are $P_2(-x_7,y_3)$, $P_3(-x_7, -y_3)$ and $P_2(x_7, -y_3)$. Numerical values of x^py^q for the points P_1, P_2, P_3 and P_4 with different possibilities of exponent indices p and q are listed in Table 1.

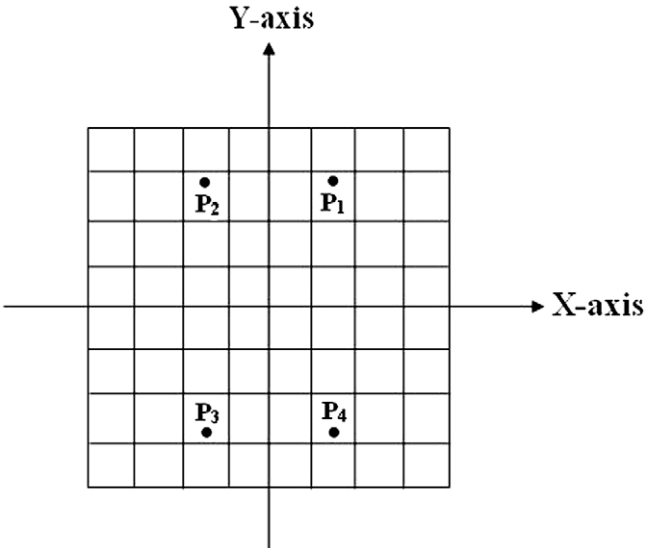

Fig. 2. The image is divided into four equal quadrants.

Based on this symmetry property and the results obtained in Table 1, the geometric moments can then be evaluated according to the following four cases:

Case 1: p and q are both even;

$$f_k(x_i,y_j) = f_1(x_i,y_j) + f_2(x_i,y_j) + f_3(x_i,y_j) + f_4(x_i,y_j), \tag{14.1}$$

Case 2: p is even and q is odd;

$$f_k(x_i,y_j) = f_1(x_i,y_j) + f_2(x_i,y_j) - f_3(x_i,y_j) - f_4(x_i,y_j), \tag{14.2}$$

Case 3: p is odd and q is even;

$$f_k(x_i,y_j) = f_1(x_i,y_j) - f_2(x_i,y_j) - f_3(x_i,y_j) + f_4(x_i,y_j), \tag{14.3}$$

Case 4: p and q are both odd;

$$f_k(x_i,y_j) = f_1(x_i,y_j) - f_2(x_i,y_j) + f_3(x_i,y_j) - f_4(x_i,y_j). \tag{14.4}$$

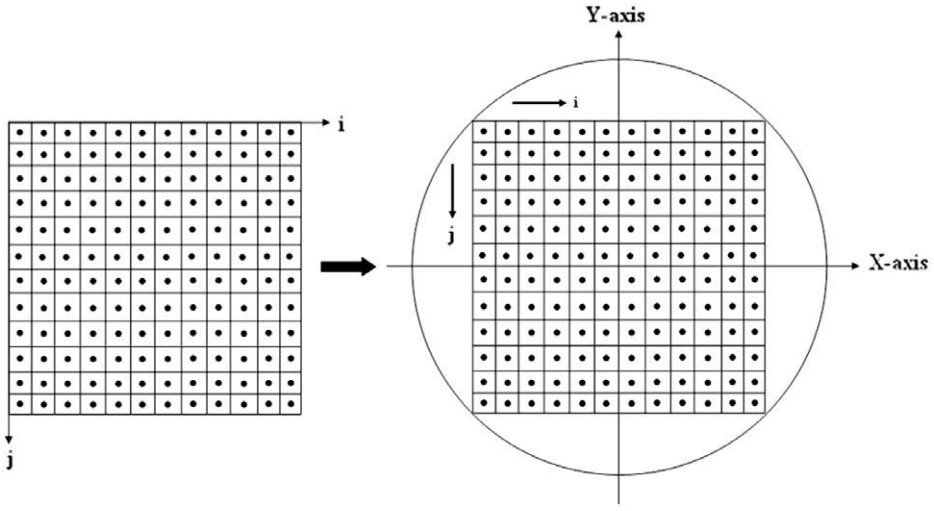

Fig. 1. The whole square image is mapped inside the unit disk.

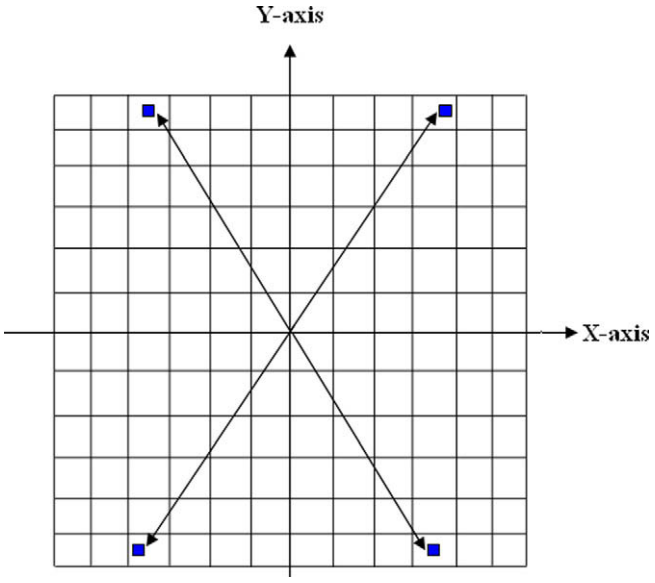

Fig. 3. Radial distances from the origin to a specific pixel in the four quadrants are equal.

Table 1
Numerical values of $x^p y^q$ are dependent on whatever p and q are even or odd.

p	q	$x^p y^q$			
		P_1	P_2	P_3	P_4
Even = 4	Even = 2	+0.000965	+0.000965	+0.000965	+0.000965
Even = 2	Odd = 1	+0.031074	+0.031074	−0.031074	−0.031074
Odd = 3	Even = 2	+0.003641	−0.003641	−0.003641	+0.003641
Odd = 3	Odd = 1	+0.008239	−0.008239	+0.008239	−0.008239

where $f_1(x_i,y_j)$ is the intensity function of the pixel point (x_i,y_j) in the first quadrant; the other functions $f_2(x_i,y_j)$, $f_3(x_i,y_j)$ and $f_4(x_i,y_j)$ are the intensity functions at the corresponding pixel points in the second, third and fourth quadrants, respectively.

3.2. Exact computation of radial moments

According to the square-to-circle transformation, the transformed image is defined in the square $\left[-1/\sqrt{2},1/\sqrt{2}\right]\times\left[-1/\sqrt{2},1/\sqrt{2}\right]$; therefore, the $(p+q)$ order geometric moments are defined as:

$$M_{pq}=\int_{-\frac{1}{\sqrt{2}}}^{\frac{1}{\sqrt{2}}}\int_{-\frac{1}{\sqrt{2}}}^{\frac{1}{\sqrt{2}}}x^p y^q f(x,y)\,dx\,dy. \tag{15}$$

Radial moments are expressed as a linear combination of geometric moments of the same order or less as follows (Hosny, 2008):

$$R_{pq}=\sum_{j=0}^{S}\sum_{m=0}^{q}w^m\binom{S}{j}\binom{q}{m}M_{p-2j-m,2j+m} \tag{16.1}$$

with

$$R_{pp}=\sum_{m=0}^{p}w^m\binom{p}{m}M_{p-m,m}, \tag{16.2}$$

where $S=(p-q)/2$, $w=-\sqrt{-1}$ if $q>0$ or $w=\sqrt{-1}$ if $q\leqslant 0$. Based on Eq. (16), exact computation of geometric moments results in exact values of radial moments. As shown in (Hosny, 2008), the time-consuming direct computations of factorial terms are avoided by using recurrence relations:

$$D_{0,0}=1, \tag{17.1}$$
$$D_{p,0}=1, \tag{17.2}$$
$$D_{p,k}=\frac{p}{p-k}D_{p-1,k}, \tag{17.3}$$
$$D_{p,k}=\frac{1}{k(p-k)}D_{p,k-1}. \tag{17.4}$$

It is clear that, the matrix D is independent on the image, where its dimensions are dependent only on the moment's order. Therefore, this matrix is pre-computed and stored for future use.

Similar to our previous work (Hosny, 2007), exact geometric moments for the whole input image could be easily obtained through the computation of the first quadrant only. This could be achieved by using the augmented intensity function $f_k(x_i,y_j)$ defined in Eq. (14). As discussed in the previous section, the augmented intensity function has four different values based on whatever the indices p and q are even or odd as follows:

$$\widehat{M}_{pq}=\sum_{i=1}^{\left\lfloor\frac{N}{2}\right\rfloor}\sum_{j=1}^{\left\lfloor\frac{N}{2}\right\rfloor}I_p(i)I_q(j)f_k(x_i,y_j), \tag{18}$$

where

$$\left\lfloor\frac{N}{2}\right\rfloor=\begin{cases}(N-1)/2, & N\text{ is odd},\\ N/2, & N\text{ is even}.\end{cases} \tag{19}$$

Implementation of Eq. (18) results in the reduction of the computational cost by 75%, where only one quadrant is considered. For more details about computational complexity, the reader is advised to read Section 4.2. The kernels $I_p(i)$ and $I_q(j)$ are defines as follows:

$$I_p(i)=\frac{1}{p+1}\left[U_{i+1}^{p+1}-U_i^{p+1}\right], \tag{20.1}$$
$$I_q(j)=\frac{1}{q+1}\left[V_j^{q+1}-V_{j+1}^{q+1}\right] \tag{20.2}$$

with

$$U_{i+1}=x_i+\frac{\Delta x_i}{2}, \tag{21.1}$$
$$U_i=x_i-\frac{\Delta x_i}{2}, \tag{21.2}$$
$$V_{j+1}=y_j+\frac{\Delta y_j}{2}, \tag{21.3}$$
$$V_j=y_j-\frac{\Delta y_j}{2}. \tag{21.4}$$

The time complexity of Eq. (18) could be significantly reduced by successive computation of the 1D qth order moments for each row. Eq. (18) will be rewritten in the following separable form:

$$\widehat{M}_{pq}=\sum_{i=1}^{\left\lfloor\frac{N}{2}\right\rfloor}I_p(i)Y_{iq}, \tag{22}$$

where

$$Y_{iq}=\sum_{j=1}^{\left\lfloor\frac{N}{2}\right\rfloor}I_q(j)f_k(x_i,y_j). \tag{23}$$

$Y_{i\,q}$ in Eq. (23) is the qth order moment of row i. Since,

$$I_0(i)=\sqrt{2}/N. \tag{24}$$

Substitute Eq. (24) into Eq. (18), yields:

$$\widehat{M}_{0q}=\frac{\sqrt{2}}{N}\sum_{i=1}^{\left\lfloor\frac{N}{2}\right\rfloor}Y_{iq}. \tag{25}$$

4. Numerical experiments

In this section, the validity proof of the proposed method will be presented. Artificial test images are used in our numerical experiments where, radial moments that are computed using the proposed method are compared with theoretical and ZOA approximate values. Both ZOA and Wee's method (Wee and Paramesran, 2006), are used to approximately compute a set of radial moments, where the later one was derived from the same formula of ZOA method. The artificial test images are relatively small so that hand calculations can be easily employed. CPU elapsed time for real standard images are used to compare the required computational time of the proposed method against ZOA and Wee's method.

4.1. Artificial test images

4.1.1. First image

Artificial test images of small size are used to prove validity of the proposed method, where hand calculations could be employed and the theoretical values easily obtained. A special image with intensity function, $f(x,y) = 1$ for all points (x,y) is considered. The size of this artificial test images is 4×4. The original image that is defined in the square $[-1,1] \times [-1,1]$ is mapped to be inside the unit circle, where the coordinate origin is the center of the circle. The image center coincides with the circular center. The mapped image is defined in the square $\left[-1/\sqrt{2}, 1/\sqrt{2}\right] \times \left[-1/\sqrt{2}, 1/\sqrt{2}\right]$. Consequently, the set of two-dimensional geometric moments of order $(p+q)$ are:

$$M_{pq} = \left(\frac{\left(1/\sqrt{2}\right)^{p+1} - \left(-1/\sqrt{2}\right)^{p+1}}{p+1} \right) \left(\frac{\left(1/\sqrt{2}\right)^{q+1} - \left(-1/\sqrt{2}\right)^{q+1}}{q+1} \right). \tag{26}$$

Eq. (26) can be simplified as follows:

$$M_{pq} = \begin{cases} \frac{4\left(1/\sqrt{2}\right)^{p+q+2}}{(p+1)(q+1)}, & p = \text{even}, \\ 0, & p = \text{odd}. \end{cases} \tag{27}$$

In this case, theoretical values of radial moments are calculated by using Eq. (27) into Eq. (16). The corresponding exact values are calculated using Eqs. (22)–(25) and (14) in Eq. (16). The ZOA approximated values using Eq. (2). It is clear that exact and theoretical values are identical. For quick comparison, all calculated values are shown in Table 2.

4.1.2. Second image

The intensity function of the second artificial test image is represented by the matrix: $A = [3,2,1,5;6,1,7,3;2,8,4,6;5,1,4,2]$. Radial moments for this image are shown in Table 3. It is obvious that the computed values using the proposed method are identical to theoretical values, while the approximate ZOA values deviate from the theoretical values especially when the moment order increases, see Table 3.

Table 2
Comparison of theoretical, R_{pq}, exact, $\widehat{R}_{pq}$, and ZOA, $\widetilde{R}_{pq}$ for $f(x_i,y_j) = 1$.

p	q	Theoretical, R_{pq}	Exact, $\widehat{R}_{pq}$	ZOA, $\widetilde{R}_{pq}$
0	0	2.0007	2.0007	2.0007
1	0	0.0000	0.0000	0.0000
1	1	0.0000	0.0000	0.0000
2	0	0.6666	0.6666	0.6250
2	1	0.3333	0.3333	0.3125
2	2	0.0000	0.0000	0.0000
3	0	0.0000	0.0000	0.0000
3	1	0.0000	0.0000	0.0000
3	2	0.0000	0.0000	0.0000
3	3	0.0000	0.0000	0.0000
4	0	0.3111	0.3111	0.2578
4	1	0.1555	0.1555	0.1289
4	2	0.0000	0.0000	0.0000
4	3	−0.066	−0.066	−0.0664
4	4	−0.1333	−0.1333	−0.1328
5	0	0.0000	0.0000	0.0000
5	1	0.0000	0.0000	0.0000
5	2	0.0000	0.0000	0.0000
5	3	0.0000	0.0000	0.0000
5	4	0.0000	0.0000	0.0000
5	5	0.0000	0.0000	0.0000
6	0	0.1714	0.1714	0.1196
6	1	0.0857	0.0857	0.0598
6	2	0.0000	0.0000	0.0000
6	3	−0.0476	−0.0476	−0.0402
6	4	−0.0952	−0.0952	−0.0805
6	5	−0.0476	−0.0476	−0.0402
6	6	0.0000	0.0000	0.0000

Table 3
Comparison of theoretical, R_{pq}, exact, $\widehat{R}_{pq}$, and ZOA, $\widetilde{Z}_{pq}$ for $f(x_i,y_j) = A$.

p	q	Theoretical, R_{pq}	Exact, $\widehat{R}_{pq}$	ZOA, $\widetilde{Z}_{pq}$
0	0	7.5000	7.5000	7.5000
1	0	0.1325	0.1325	0.1325
1	1	0.1325 − 0.0883i	0.1325 − 0.0883i	0.1325 − 0.0883i
2	0	2.3437	2.3437	2.3437
2	1	1.0312 + 0.0859i	1.0312 + 0.0859i	0.9531 + 0.0859i
2	2	−0.2812 + 0.1718i	−0.2812 + 0.1718i	−0.2812 + 0.1718i
3	0	0.0082	0.0082	0.0027
3	1	0.0082 − 0.0036i	0.0082 − 0.0036i	0.0076 − 0.0022i
3	2	0.0414 + 0.0036i	0.0414 + 0.0036i	0.0386 + 0.0055i
3	3	0.0745 + 0.0110i	0.0745 + 0.0110i	0.0745 + 0.0110i
4	0	1.0950	1.0950	0.9082
4	1	0.4947 + 0.0664i	0.4947 + 0.0664i	0.4101 + 0.0610i
4	2	−0.1054 + 0.1328i	−0.1054 + 0.1328i	−0.0878 + 0.1220i
4	3	−0.3125 + 0.0839i	−0.3125 + 0.0839i	−0.3027 + 0.0786i
4	4	−0.5195 + 0.0351i	−0.5195 + 0.0351i	−0.5175 + 0.0351i
5	0	−0.0092	−0.0092	−0.0098
5	1	−0.0092 + 0.0098i	−0.0092 + 0.0098i	−0.0098 + 0.0100i
5	2	0.0154 + 0.0121i	0.0154 + 0.0121i	0.0120 + 0.01173i
5	3	0.0401 + 0.0143i	0.0401 + 0.0143i	0.0340 + 0.0134i
5	4	0.0266 − 0.0098i	0.0266 − 0.0098i	0.0236 − 0.0103i
5	5	0.0131 − 0.0340i	0.0131 − 0.0340i	0.0132 − 0.0341i
6	0	0.61209	0.61209	0.42968
6	1	0.2845 + 0.0536i	0.2845 + 0.0536i	0.2011 + 0.0431i
6	2	−0.0430 + 0.1073i	−0.0430 + 0.1073i	−0.0274 + 0.0863i
6	3	−0.2037 + 0.0610i	−0.2037 + 0.0610i	−0.1675 + 0.0486i
6	4	−0.3644 + 0.0146i	−0.3644 + 0.0146i	−0.3076 + 0.011i
6	5	−0.1756 − 0.0684i	−0.1756 − 0.0684i	−0.1477 − 0.0699i
6	6	0.0131 − 0.1514i	0.0131 − 0.1514i	0.0121 − 0.1508i

4.2. Computational complexity

Complexity analysis of the considered methods is very important, where such analysis give a simple and clear way to judge the efficiency of the different methods. Complexity analysis mainly concentrates on the number of multiplications and additions required by each method. Evaluation of factorial terms, exponential and power functions are considered if encounter in any one of the considered methods. For a gray-level image of size $N \times N$ and a maximum moment order equal to *Max*, the analysis of the direct ZOA approximation method represented by Eq. (2) is discussed first. Computation of an individual radial moment required the evaluation of the power function r_{ij}^{p} and the exponential function $e^{-\mathrm{i}q\theta_{ij}}$ plus six multiplication process. Three are included in the evaluation of the exponential function and the rest are a result of multiplying both power and exponential function with the image

Table 4
Complexity analysis of radial moment's computation methods: for gray-level image of size $N \times N$ and a maximum moment order equal to *Max*.

	ZOA method	Wee's method (2006)	Proposed method
Multiplications	$6N^2(Max+1)^2$	$6(N/2)^2(Max+1)^2$	$\frac{(Max+1)}{4}\left[N^2+NMax+4\right]+(Max+1)(Max+2)+3Max\lfloor Max/2\rfloor\lfloor(Max+1)/2\rfloor$
Additions	$N^2(Max+1)^2/2$	$(N/2)^2(Max+1)^2/2$	$\frac{(Max+1)}{4}\left[N^2-4+Max(N-2)\right]+Max(Max+1)/2+(Max-1)\lfloor Max/2\rfloor\lfloor(Max+1)/2\rfloor$
Power functions	$N^2(Max+1)^2$	$(N/2)^2(Max+1)^2$	–
Exponential functions	$N^2(Max+1)^2$	$(N/2)^2(Max+1)^2$	–

Table 5
Complexity analysis of geometric moment's computation methods: for gray-level image of size $N \times N$ and a maximum moment order equal to *Max*.

GM	Multiplications	Additions
ZOA method	$(Max+1)(Max+2)N^2$	$\frac{(Max+1)(Max+2)}{2}N^2$
Wee's method (2008)	$(Max+1)(Max+2)\left(\frac{N}{2}\right)^2$	$\frac{(Max+1)(Max+2)}{2}\left(\frac{N}{2}\right)^2$
Hosny's method (2007)	$(Max+1)\left[N^2+\frac{NMax}{2}+1\right]$	$(Max+1)\left[N^2+\frac{(N-2)Max}{2}-1\right]$
Proposed method	$\frac{(Max+1)}{4}\left[N^2+NMax+4\right]$	$\frac{(Max+1)}{4}\left[N^2-4+Max(N-2)\right]$

intensity function. All of these processes are repeated for all pixels of the input image. Therefore, we could summarize the computational complexity of the direct method as $6N^2(Max+1)^2$ multiplications, $N^2(Max+1)^2/2$ additions, $N^2(Max+1)^2$ power functions and finally $N^2(Max+1)^2$ exponential functions.

Complexity analysis of the approximation method of (Wee and Paramesran, 2006) is very similar to the direct method except the implementation of the symmetrical property to compute radial moment functions in the first quadrant and then obtained the radial moment functions of the other three octants straightforward. Unfortunately, radial moment's computation by using the method of Wee and Paramesran required the evaluation of both power and exponential functions. The method of (Wee and Paramesran, 2006) required $6(N/2)^2(Max+1)^2$ multiplications, $(N/2)^2(Max+1)^2/2$ additions, evaluation of $(N/2)^2(Max+1)^2$ power functions and finally $(N/2)^2(Max+1)^2$ exponential function evaluation.

The proposed method consists of two main steps. First one is the exact computation of geometric moments and the second is the radial moment's computation as a linear combination of geometric moments. The number of independent geometric moments for a maximum order *Max* is $(Max+1)(Max+2)/2$. The complexity analysis of exact geometric moment's computation by using Eqs. (22), (23) and (25) is discussed in details. Creation of the matrix $Y_{i\ q}$ in Eq. (23) requires $(N/2)^2(Max+1)$ additions and $(N/2)^2(Max+1)$ multiplications. First row computation of geometric moments using Eq. (25) requires $(N/2-1)(Max+1)$ additions and $(Max+1)$ multiplications. The rest of geometric moments are computed using Eq. (22) which requires $(N/2-1)(Max/2)(Max+1)$ additions and $(N/2)(Max/2)(Max+1)$ multiplications.

The complexity analysis of radial moment's computation as a linear combination of geometric moments by using Eqs. (16.1) and (16.2) are divided into two stages. First one concerned with Eq. (16.2) which requires $Max(Max+1)/2$ additions and $(Max+1)(Max+2)$ multiplications. The second stage represented by Eq. (16.1) that requires $(Max-1)\lfloor Max/2\rfloor\lfloor(Max+1)/2\rfloor$ and $3Max\lfloor Max/2\rfloor\lfloor(Max+1)/2\rfloor$ multiplications, where the operator $\lfloor\bullet\rfloor$ is defined using Eq. (19).

Complexity analysis of the direct ZOA (Wee and Paramesran, 2006) and the proposed methods are summarized in Table 4. It is easy to compare these three methods. For $N=512$ and $Max=55$, the direct ZOA (Wee and Paramesran, 2006) and the proposed method requires 4932501504, 1233125376 and 4192244 multiplications, respectively. These methods require 411041792, 102760448 and 4105024 additions, respectively. The reader must notice that, the power and exponential functions are excluded from the comparison. It is obvious that, the proposed method tremendously reduces the computational complexity.

The proposed method includes a modified algorithm for fast computation of geometric moments. To clearly demonstrate the efficiency of this method, a complexity analysis of it is compared with the existing methods like, direct ZOA (Hosny, 2007; Wee et al., 2008). Table 5 shows the number of multiplications and additions required by each of the aforementioned methods. A

Fig. 4. Test images: (a) peppers and (b) boat.

quick comparison of these four methods could be done for $N = 512$ and $Max = 55$, the direct ZOA (Wee et al., 2008; Hosny, 2007) and the proposed method require 836763648, 209190912, 16257080 and 4064312 multiplications, respectively. These methods require 418381824, 104595456, 15465408 and 4062660 additions, respectively. It is clear that, the proposed method is the most efficient one.

4.3. Computational time

The main drawback of using circularly moments is their consuming computational time. Therefore, computational time reduction is a very important issue especially for large size images and objects. The CPU elapsed time is used in the comparison process in all the performed numerical experiments. All our numerical experiments are performed with 1.8 GHz Pentium IV PC with 512 MBYTE RAM. The executed code is designed by using MATLAB7. The set of radial moments is computed by using the proposed method, the method of (Wee and Paramesran, 2006) and the approximation ZOA method. In the first experiment, a gray-scale image of peppers with size 128×128 as in Fig. 4a is used. The CPU elapsed times for the three different methods are included in Table 6. It is clear that, the proposed method reduce the execution time tremendously.

In the second numerical experiment, the set of radial moments are computed for the boat test images with size 512×512. This test image is relatively large. The CPU elapsed times are graphically represented Fig. 5. Tables 7 shows the elapsed times of the different methods for a selected moment orders. Similar to results of the previous numerical experiments the execution time of ZOA and Wee's methods monotonically increase as the moment order increase, while the execution time required by the proposed method is extremely small. Based on the obtained results we conclude that, both ZOA and Wee's methods are impractical for large images and moments with higher orders.

Table 6
CPU elapsed time in seconds for the 128×128 pepper's gray-scale test image.

Moment order	ZOA method	Wee' method (2006)	Proposed method
$Max = 5$	0.7340	0.203000	0.016000
$Max = 15$	7.4370	2.047000	0.047000
$Max = 25$	23.6100	5.703000	0.110000
$Max = 35$	53.0310	11.87500	0.219000
$Max = 45$	91.9690	22.34400	0.453000
$Max = 55$	137.8600	36.06300	0.860000
$Max = 65$	193.4380	51.98500	1.531000

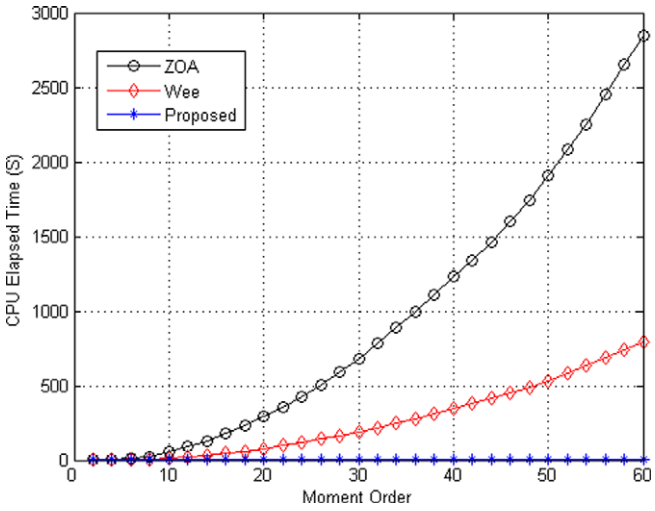

Fig. 5. Linear scale of CPU elapsed time in seconds for the 512×512 gray-scale boat image

Table 7
CPU elapsed time in seconds for the 512×512 boat's gray-scale test image.

Moment order	ZOA method	Wee's method (2006)	Proposed method
$Max = 5$	14.0620	4.141000	0.859000
$Max = 15$	177.5310	44.922000	1.312000
$Max = 25$	501.5780	141.407000	1.797000
$Max = 35$	991.7030	278.187000	2.438000
$Max = 45$	1596.9680	455.672000	3.219000
$Max = 55$	2452.4530	690.047000	4.328000

The obtained results in this section clearly shows that, our proposed method is accurate where the set of radial moments are computed exactly using a set of exact geometric moments, while, on the other side, Wee's method is inaccurate where the set of radial moments are computed approximately. The comparison of the CPU elapsed times ensures the superiority of the proposed method against Wee's method, where the proposed method extremely reduces the execution times.

5. Conclusion

This work proposes fast, accurate and low-complexity method of radial moment computation for gray-scale images. Due to the wide range of their applications, the accurate computation of circular moments is a very crucial problem. Based on their relation with the geometric moments, radial moments are computed exactly. Consequently, the set of circular moments could be accurately computed based on their representation as a linear combination of radial moments. The implementation of the symmetry property significantly reduces the computational complexity demands. The numerical experiments are performed for real images with different sizes to ensure the efficiency of the proposed method.

References

Amin, P., Subhulukshini, K.E., 2004. Rotation and cropping resilient data hiding with Zernike moments. Internat. Conf. Image Process., 2175–2178.
Bharathi, V.S., Ganesan, L., 2008. Orthogonal moments based texture analysis of CT liver images. Pattern Recognition Lett. 29, 1868–1872.
Bin, T.J., Lei, A., Wen, C.J., Wen-jing, K., Dan-dan, L., 2008. Subpixel edge location based on orthogonal Fourier-Mellin moments. Image Vision Comput. 26, 563–569.
Broumandnia, A., Shanbehzadeh, J., 2007. Fast Zernike wavelet moments for Farsi character recognition. Image Vision Comput. 25, 717–726.
Dong, Q.Y., Song, C.C., Ben, C.S., Quan, L.J., 2005. A fast subpixel edge detection method using Sobel–Zernike moments operator. Image Vision Comput. 23, 11–17.
Ghosal, S., Mehrotra, R., 1992. Edge detection using orthogonal moment-based operators. In: Proc. 11th Internat. Conf. on Pattern Recognition, pp. 413–416.
Ghosal, S., Mehrotra, R., 1993. Segmentation of range images: an orthogonal moment-based integrated approach. IEEE Trans. Robot. Automat. 9, 385–399.
Haddadnia, J., Ahmadi, M., Faez, K., 2003. An feature extraction method with pseudo-Zernike moments in RBF neural network-based human face recognition system. EURASIP J. Appl. Signal Process. 9, 890–901.
Hosny, K.M., 2007. Exact and fast computation of geometric moments for gray level images. Appl. Math. Comput. 189, 1214–1222.
Hosny, K.M., 2008. Fast computation of accurate Zernike moments. J. Real-Time Image Process. 3, 97–107.
Iskander, D.R., Collins, M.J., Davis, B., 2001. Optimal modeling of corneal surfaces with Zernike polynomials. IEEE Trans. Biomed. Eng. 48, 87–95.
Iskander, D.R., Morelande, M.R., Collins, M.J., Davis, B., 2002. Modelling of corneal surfaces with radial polynomials. IEEE Trans. Biomed. Eng. 49, 320–328.
Kan, C., Srinath, M.D., 2002. Invariant character recognition with Zernike and orthogonal Fourier-Mellin moments. Pattern Recognition 35, 143–154.
Kanan, H.R., Faez, K., 2009. GA-based optimal selection of PZMI features for face recognition. Appl. Math. Comput. 205, 706–715.
Khotanzad, A., Hong, Y.H., 1990. Invariant image recognition by Zernike moments. IEEE Trans. Pattern Anal. Machine Intell. 12, 489–497.
Kim, H.S., Lee, H.K., 2003. Invariant image watermark using Zernike moments. IEEE Trans. Circuits Systems Video Technol. 13, 766–775.

Kim, W.Y., Kim, H.J., 2008. Eye detection in facial images using Zernike moments with SVM. ETRI J. 30, 335–337.
Kim, Y.S., Kim, W.Y., 1998. Content-based trademark retrieval system using visually salient feature. Image Vision Comput. 16, 931–939.
Novotni, M., Klein, R., 2004. Shape retrieval using 3D Zernike descriptors. Comput. Aided Des. 36 (11), 1047–1062.
Sheng, Y., Shen, L., 1994. Orthogonal Fourier-Mellin moments for invariant pattern recognition. J. Opt. Soc. Amer. A 11, 1748–1757.
Teague, M.R., 1980. Image analysis via the general theory of moments. J. Opt. Soc. Amer. A 7, 920–930.
Teh, C.H., Chin, R.T., 1988. On image analysis by the method of moments. IEEE Trans. Pattern Anal. Machine Intell. 10, 496–513.
Wang, L., Healey, G., 1998. Using Zernike moments for the illumination and geometry invariant classification of multispectral texture. IEEE Trans. Image Process. 7, 196–203.
Wee, C.Y., Paramesran, R., 2006. Efficient computation of radial moment functions using symmetrical property. Pattern Recognition 39, 2036–2046.
Wee, C.-Y., Paramesran, R., Mukundan, R., 2008. Fast computation of geometric moments using a symmetric kernel. Pattern Recognition 41, 2369–2380.
Xin, Y., Liao, S., Pawlak, M., 2004. Geometrically robust image watermarking via pseudo-Zernike moments. In: Proc. 2004 Canad. Conf. on Electrical and Computer Engineering, pp. 939–942.